Chapter 5

Overall Properties of GaAsN/GaAs MQWs, As Grown and After Annealing

5.1 Experimental Setup

Molecular Beam Epitaxy (MBE) All the samples under study were grown by radio-frequency plasma-assisted molecular beam epitaxy (RF-MBE). Fig. 5.1 shows a schematic view of the growth chamber of the MBE machine. An RF-MBE apparatus is equipped with:

1. A sample holder which can rotate around an axis parallel to the growth direction, and whose temperature can be controlled
2. Effusion cells which are the source of Ga and As
3. A radio frequency plasma source which supplies the nitrogen for the sample growth. Microwave radiation with a frequency of 13.56 MHz is coupled to a cavity to convert an ultrapure molecular nitrogen flow into atomic nitrogen.
4. Reflection high energy electron diffraction(RHEED) system: this includes an upper RHEED gun and a RHEED camera below which are used for *in situ* monitoring of the growing surface

During the growth, the MBE chamber is under ultra high vacuum (UHV) of about 10^{-10} mbar.

Photoluminescence In the PL measurement, the excitation laser was derived from a tunable Coherent Ti:sapphire laser (Model 890) with an excitation energy of E_{exc}=1.59 eV, which is pumped by a Coherent Verdi V-5 (frequency-doubled Nd:YAG) laser. For sufficient stray light suppression, the PL emission signal was dispersed in a 1-m triple monochromator. The output signal was recorded by an LN-cooled InGaAs array detector.

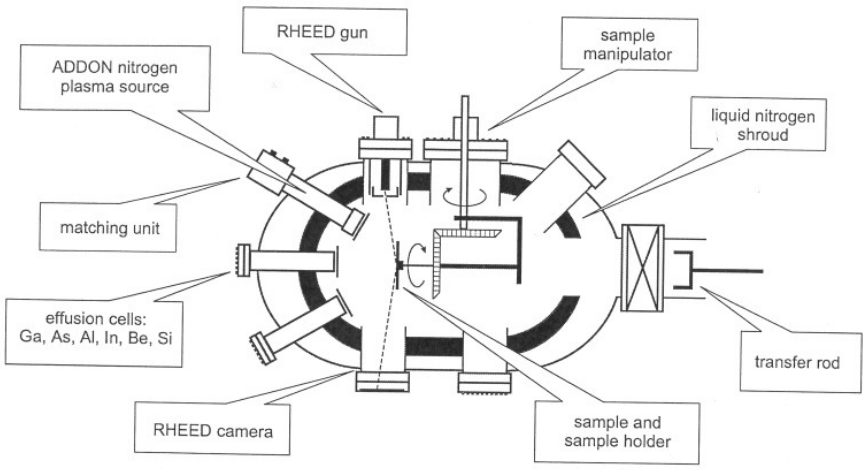

Figure 5.1: Schematic view of the MBE growth chamber

Raman Scattering Raman scattering (RS) spectra were taken in a backscattering configuration from the epilayer surface. The scattered light was analyzed by a LABRAM single spectrograph equipped with a cooled charge-coupled device array. A He-Ne laser line at 633 nm wavelength was used for the optical excitation.

A polarization rotator and an analyzer were used to examine the allowed $z(x,y)\bar{z}$ and $z(x,x)\bar{z}$ light. Here, z and $\bar{z}$ represent the incident and scattered light directions (001) and $(00\bar{1})$, while $x = (110)$ and $y = (1\bar{1}0)$ correspond to the light polarization directions. The experiments were carried out at room temperature.

Transmission Electron Microscopy (TEM) The TEM images were recorded with a high resolution JEOL 3010 microscope equipped with a Gatan slow scan charge-coupled device camera. The cross-sectional specimens were prepared by standard mechanical polishing followed by Ar^+ ion milling.

Rapid Thermal Annealing (RTA) The RTA processes were carried out using a Jetfirst 100 furnace. The annealing was implemented in an N_2 ambient atmosphere with a controlled temperature ramp of 20 K/s. In order to avoid arsenic desorption, the samples were proximity capped with a GaAs wafer.

X-Ray Diffraction XRD measurements were carried out on a Philips instrument. The experimental results were simulated using a dynamical XRD analysis model which is suitable for accurately determining the compositions of highly mismatched materials systems [74].

5.2 Sample Growth

The samples under study were grown using a solid-source molecular-beam epitaxy (MBE) system. Nitrogen was supplied by an RF plasma source. Ga(As,N) samples

with nitrogen concentrations of 0.6%, 2.2%, 3%, 4%, 5%, and 6.1%, (determined by XRD $2\theta - \omega$ scan dynamic simulation) consist of a 10-period $(d/2d)$ Ga(As,N)/GaAs multi-quantum well (MQW) structure capped with 50+nm GaAs. The thickness of the well layer was $d \approx 10nm$. The Ga(As,N) well thickness d was chosen to be sufficiently small to avoid a roughening of the samples (d decreases slightly with increasing N concentration.)

Nitrogen was supplied by an Addon rf plasma source. Prior to GaAsN growth, a 400 nm GaAs buffer layer was deposited at 550°C. To ignite the plasma source, the process was interrupted for 10 min in between buffer-layer and GaAsN growth. The 100 nm film is subsequently grown at 450°C with a growth rate of 0.13 monolayers per second. The plasma source parameters are 220 W and 0.015 sccm. Finally, the samples were capped with 50 nm GaAs grown at 450°C. The reflection high-energy electron diffraction (RHEED) pattern indicates a transition from a (2X4) surface reconstruction during buffer-layer growth to a (2X3) surface reconstruction mode during the GaAsN and capping layer growth processes. The structure of the samples is shown in Fig. 5.2

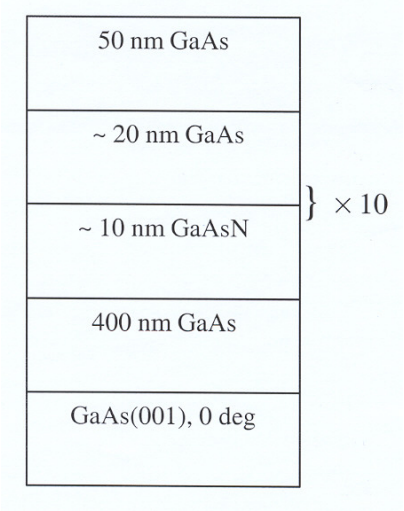

Figure 5.2: Structure of the GaAsN/GaAs MQW samples

5.3 Overall Properties of the Samples

5.3.1 Structural Properties of GaAsN/GaAs Multiquantum Well (MQW) Samples Characterized by XRD

The structural properties of GaAsN/GaAs MQW were investigated by using high-resolution X-ray diffraction (HRXRD). Fig. 5.3 shows HRXRD spectra of the GaAsN/GaAs MQW with 3% N, for the as-grown sample and the samples after undergoing RTA at 750, 800, 850 and 900°C for 60 s. The observed sharp and well-defined satellite peaks in the XRD pattern of the as-grown sample imply a coherent periodicity of the GaAsN/GaAs heterostructure and suggest the presence of very sharp interfaces.

There is an increasing broadening of the satellite peaks with increasing RTA temperature. This indicates a change in the alloy homogeneity with increasing annealing temperatures. In particular, the Pendellösung fringes which are clearly observed in the XRD curve of the as-grown sample became gradually blurred with increasing RTA temperature and eventually disappear in the XRD curve of the RTA samples at 900°C, showing that the sharp superlattice interfaces degraded after annealing. This may indicate that there is interdiffusion of elements across the interfaces. As no change of the period of the satellite peaks was demonstrated, it can be concluded that the RTA process did not affect the layer thickness.

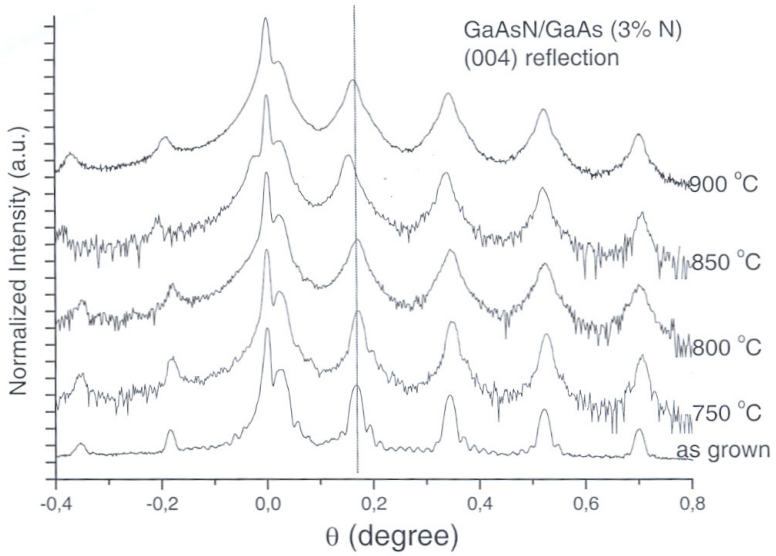

Figure 5.3: XRD pattern around the (004) reflection for a GaAsN/GaAs MQW sample with nitrogen composition of 3%, as grown and after rapid thermal annealing at different temperatures.

The separation between the main peak (GaAs substrate) and the first-order satellite peak characterizes the average MQW mismatch caused by the tetragonal extensive deformation and permits a determination of the In and N molar fractions in the wells [75]. As seen in Fig. 5.3, there is no obvious change of the tensile strain after RTA up to 800°C. At 850°C, there is a clear decrease of the tensile strain as observed in the XRD results. At 900°C, the tensile strain increased slightly compared with that at 850°C.

5.3.2 Optical Properties of GaAsN/GaAs MQWs

Recombination Mechanisms in GaAsN/GaAs MQW after RTA with N Concentrations from 0.6% to 6.1%

Figs. 5.4 and 5.5 show the excitation power dependence and temperature dependence of the photoluminescence (PL) spectra of GaAsN/GaAs MQWs with an N concentration of 3% annealed at 750°C. From Fig. 5.4, it can be seen that under low excitation power, the spectrum is composed of a high energy emission with a low energy band tail. The high energy emission results from the band-edge free-exciton recombination, while the low energy band tail is from localized states caused by N composition fluctuations. With an increase in the excitation power, the localized states saturated grad-

ually. When the excitation power reaches 16 mW, the peak from the band-edge free-exciton recombination dominates the spectrum. At the same time, with an increase of the excitation power, the emission from the band-edge free-exciton recombination shows some blue shift. In the T-PL spectra in Fig. 5.5, two peaks, at around 1.10 eV and 1.14 eV, respectively, appear in the spectrum. At low T, T =5 K-50 K, the lower energy peak dominates the spectrum. It exhibits a red shift with increasing T and a quench of its intensity with increasing T up to 50 K, which is a thermal behavior characteristic of localized carrier recombination emission. At T >50 K, the peak at higher energy dominates the spectrum. The change of its position *vs.* T follows Varnish's law for T >80K, indicating that this emission originates from band edge related free-carrier recombination. Similar double-peak structure has also been observed by Luo *et al.* [76] in GaAsN/GaAs QWs with N content of 0.2% and Wang *et al.* [77] on GaAsSbN samples with Sb and N concentrations of 2.2% and 0.5%, respectively. The change of the intensity of the two emissions is caused by the thermal excitation of the localized carriers to delocalized states. The temperature at which this transfer occurs (T_{tran}) is suggested to be an indicator of the alloy uniformity [78].

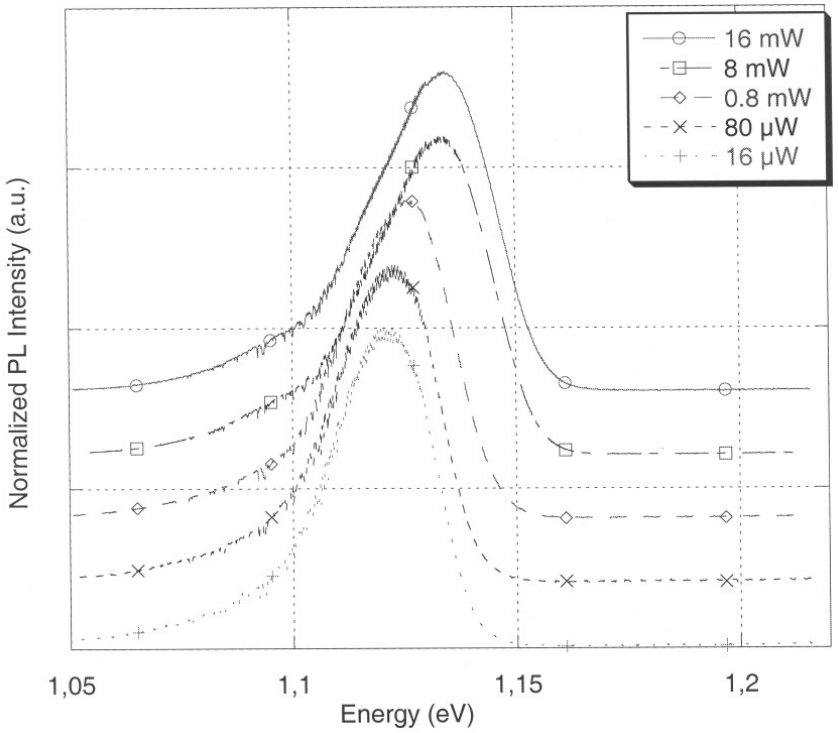

Figure 5.4: Excitation power dependent LT-PL spectra of GaAsN/GaAs MQWs with a nitrogen concentration of 3 %.

Shown in Fig. 5.6 is the temperature dependence of the PL intensity from Fig. 5.5. The integrated intensity decreased rapidly with increasing temperature (at T >180 K, the emission is too weak to discern at these temperatures). The intensity at 180 K is about 3-4 orders of magnitude lower than that at 5 K, meaning that non-radiative recombination processes were activated when the carriers were thermally excited out of the localization traps [79–82].

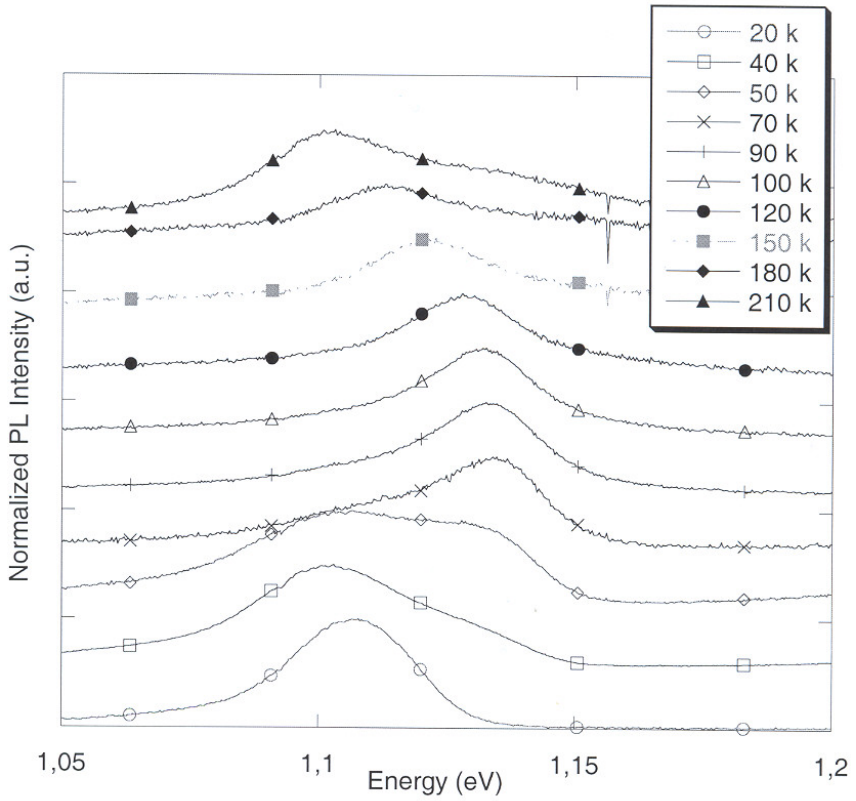

Figure 5.5: Temperature-dependent PL spectra of GaAsN/GaAs MQWs with a nitrogen concentration of 3 %.

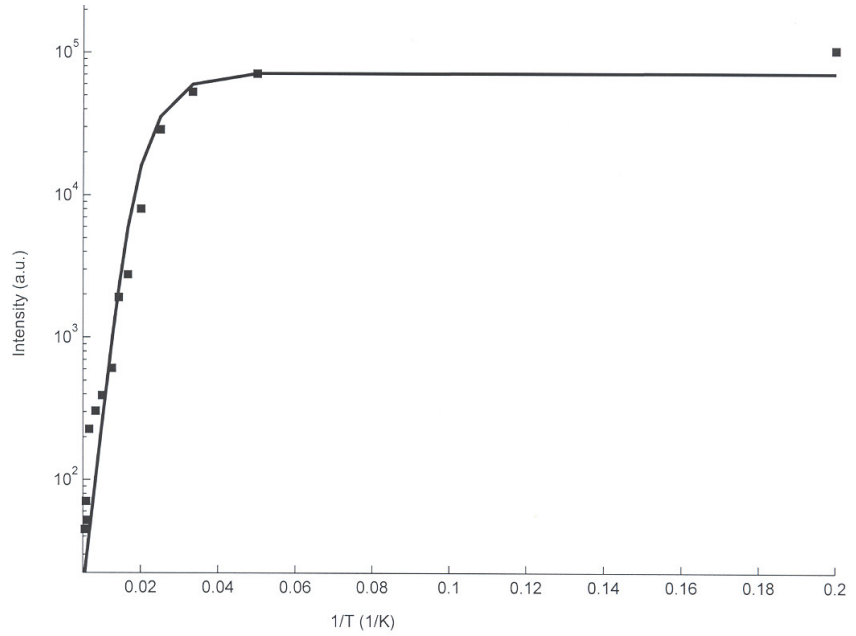

Figure 5.6: Temperature dependence of PL intensity for GaAsN/GaAs MQWs with a N concentration of 3%, RTA at 750°C

The non-radiative recombination processes have been described by [79,82]:

$$I(T) = I_0 \frac{1}{1 + Aexp(\frac{-E_a}{kT}) + Bexp(\frac{-E_b}{kT})} \tag{5.1}$$

In equation 5.1, I_0, A and B are constants, and E_a and E_b are the activation energies of the non-radiative recombination channels. By fitting our experimental results with equation 5.1, we obtained $E_a = 16$ meV $E_b = 48$ meV. (Shown in Fig. 5.6; the solid squares are the experimental data and the solid line is the simulation result). These results are close to those obtained with GaInP disordered alloys [79,82]. E_a is supposed to be related to the thermal activation of the neighboring non-radiative recombination centers, and E_b may be related to deep acceptor levels or to vacancies.

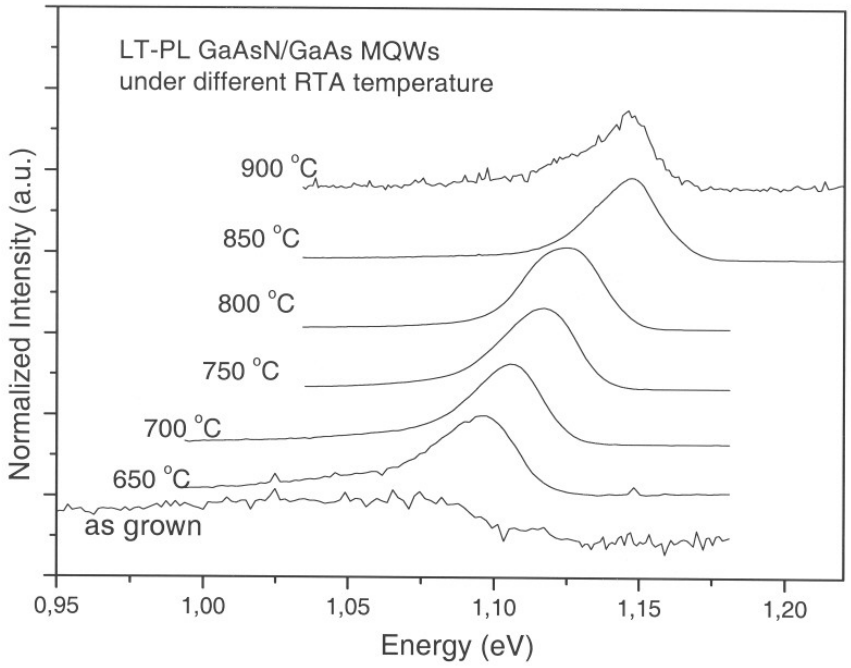

Figure 5.7: LT-PL spectra of GaAsN/GaAs MQWs with an N concentration of 3%, after RTA treatment at different temperatures

Effects of RTA on the PL properties of GaAsN/GaAs MQWs

Overall structural change Fig. 5.7 shows a typical LT-PL spectrum from the GaAsN/GaAs QWs, for the as-grown sample and the samples after RTA for 60 s at different temperatures ranging from 650°C to 900°C. In fact, the RTA treatment greatly improved the optical properties of the QWs. It is difficult to detect any emission from the as-grown samples at this excitation power. In Fig. 5.8, we also show the LT-PL spectra of the GaAsN/GaAs QWs, for the as-grown sample and the samples after RTA for 60 s at 850°C. The intensity increases from 2300 for the as-grown samples to 110000 for the sample annealed at 800°C. The full width at half maximum is 75 and 25 meV respectively for these two samples. We will discuss the mechanism of the intensity change during RTA in more detail in the next chapter.

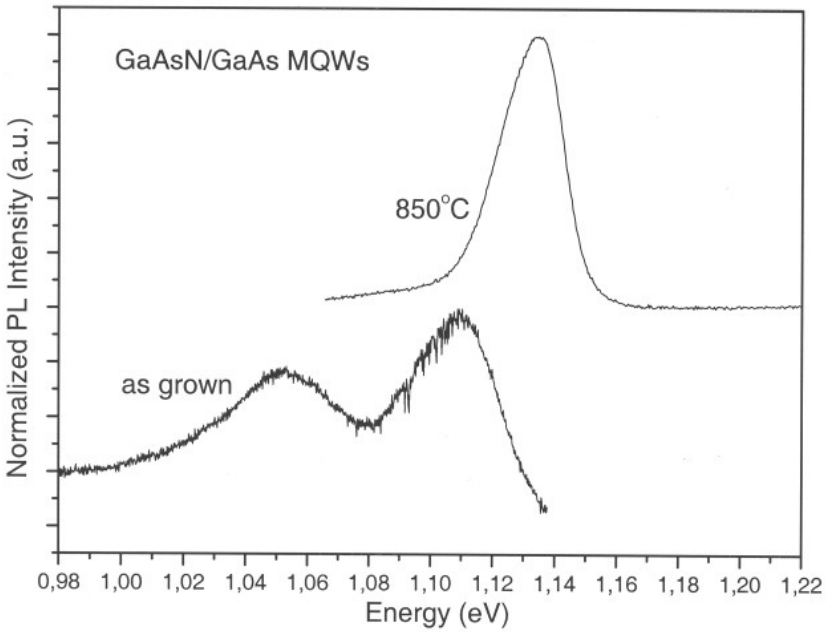

Figure 5.8: LT-PL spectra of GaAsN/GaAs MQW with an N concentration of 3%, for as-grown samples and after RTA treatment at 850°C

The PL emission wavelength also moved from 1.1 eV for as-grown samples to 1.15 eV for the samples annealed at 850°C. Although there are reports that suggested the blueshift after RTA is caused by atomic rearrangement with the well layer [45, 53], we believe that the effect of As-N interdiffusion over the well/barrier interface should not be ignored in this case, because the blueshift is too large to be interpreted as due only to atomic rearrangement [45, 47]. In order to test more directly whether there is element interdiffusion across the interface during annealing, we employed the [002] dark field [DF] technique on the MQW samples.

The [002] dark field measurement could be used to measure fairly quantitatively the element concentrations in the layers. The basic principle of this technique is:
According to the kinetic approximation, the intensity of a dark-foil d reflection (s_g=0) is given by:

$$I_g \propto t^2 F_g^2 \tag{5.2}$$

where t is the foil thickness and F_g is the structure factor for the reflection g.

For a reflection $g = (hkl)$ such as (002), for which $h + k + l = 4n + 2$, we have

$$I_g \propto t^2 [f_{Ga} - (1 - x) f_{As} - x f_N]^2 \tag{5.3}$$

for $GaAs_{1-x}N_x$
and

$$I_g \propto t^2 [f_{Ga} - f_{As}]^2 \tag{5.4}$$

for $GaAs$, where f_{Ga},f_{As} and f_N are the scattering factors for Ga,As and N respectively. So the ratio I_{GaAsN}/I_{GaAs}

$$R(x) = [(f_{Ga} - (1-x)f_{As} - xf_N) \cdot \frac{1}{f_{Ga} - f_{As}}]^2 \tag{5.5}$$

Thus, if the scattering factors of Ga,As and N are known, the ratio of the concentration of N could be derived from equation 5.5. Thus, this technique could provide relatively quantitative information on the elements' compositions. The assumption that there is an interdiffusion across the interfaces in the samples with 3% N was confirmed by the TEM (002) DF observation [83]. Similar results were also observed for the sample with 6.1% N, as shown in Fig. 5.9. (The figure shows the [002] DF images of sample with 6.1% N, for the as grown sample and the sample annealed at 750°C.)

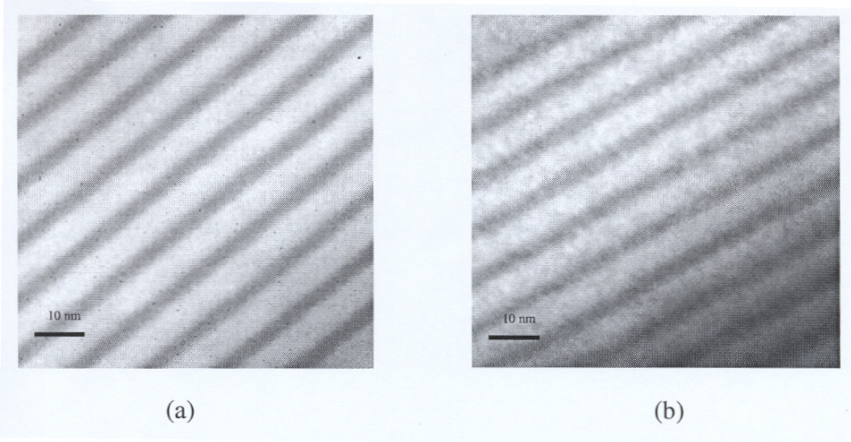

Figure 5.9: [002] dark field images of GaAsN/GaAs MQWs with an N concentration of 6.1 % (a) as grown (b) RTA at 750°C

.

Uniformity Change due to the RTA Process at Different Temperatures The temperature T_{tran} at which the transfer from localized-dominated emission to extended-dominated emission occurs is suggested to be a mark of the well layer uniformity. We studied the uniformity change at different RTA temperatures by referring to this temperature. Fig. 5.10 shows the temperature at which the transfer from the localized states to extended states occurs (for the sample with 1.25% N). T_{tran} decreases with increasing RTA temperature up to a critical temperature T_c, while at temperatures higher than T_c (850°C), it remains almost the same as at 800°C. It could be clearly derived from this that with increasing RTA temperature, the density of states in the potential fluctuation minima decreases up to T_c.

Although the localized structure is not known exactly, increase of the RTA temperature below T_c enhanced the lateral movement of N atoms and decreased the ΔE between the band gap of the localized structure and the extended states. The decrease of the confinement energy of the localized region can also be confirmed by the change in the energy differences between the localized emission and that from extended states, (ΔE) [60]. Fig. 5.10 also shows the change of ΔE *vs.* the RTA temperatures. The decrease of ΔE with the same step as the decrease of T_{tran} confirms the identification of the origin of the temperature-dependent PL emission in this group of materials. The less rapid

change in the alloying effects might be caused by a decrease of the N atoms' diffusivity with increasing temperature.

It is worth noting that all three samples (with N concentrations of 0.6, 2.2 and 3%) show the same change of T_{tran} and ΔE in the T-PL spectra.) The PL emission peak of the samples with N concentrations higher than 4% is too broad to distinguish the emission peaks from localized and extended states.

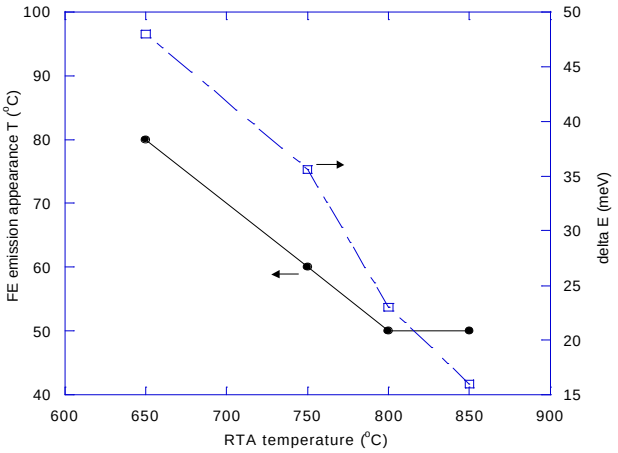

Figure 5.10: The temperature T_{tran} at which the FE emission dominates the spectrum, and the difference ΔE between the energy of the localized emission and that of the free exciton emission for GaAsN/GaAs MQWs with 1.25% N annealed under different temperatures

5.4 Strain Study by Raman Backscattering

For all the samples, the Raman spectra are well defined and there is no severe broadening shown in the spectra, which indicated that the samples retained their overall crystalline quality for the as-grown and annealed samples [84].

Fig. 5.11 shows a typical Raman spectrum of the GaAsN MQWs, here with N concentration of 2.2%, taken in the $z(x,x)\bar{z}$ scattering configuration. In these spectra, we observed a strong GaAs-like LO_1 band at 288 cm^{-1} and a TO_1 band at 266 cm^{-1}. A weak GaN-like LO_1 mode is shown at 470 cm^{-1}. The GaAs-like $2LO_1$ mode is also observed at 581 cm^{-1}. The TO phonon is observed due to relaxation of the Raman selection rule because of alloy disorder in the nitrogen-containing samples.

Fig. 5.12 shows the spectra for varying N concentrations in the GaAs LO_1 phonon range (the intensities are normalized). The linewidth of the LO_1 phonons is 4.2 cm^{-1}, comparable with the results of Prokofyeva *et al.* [84], and broader than in pure GaAs. This linewidth shows no increase with increasing N concentration, implying that the strain in the well layers is macroscopically homogeneous.

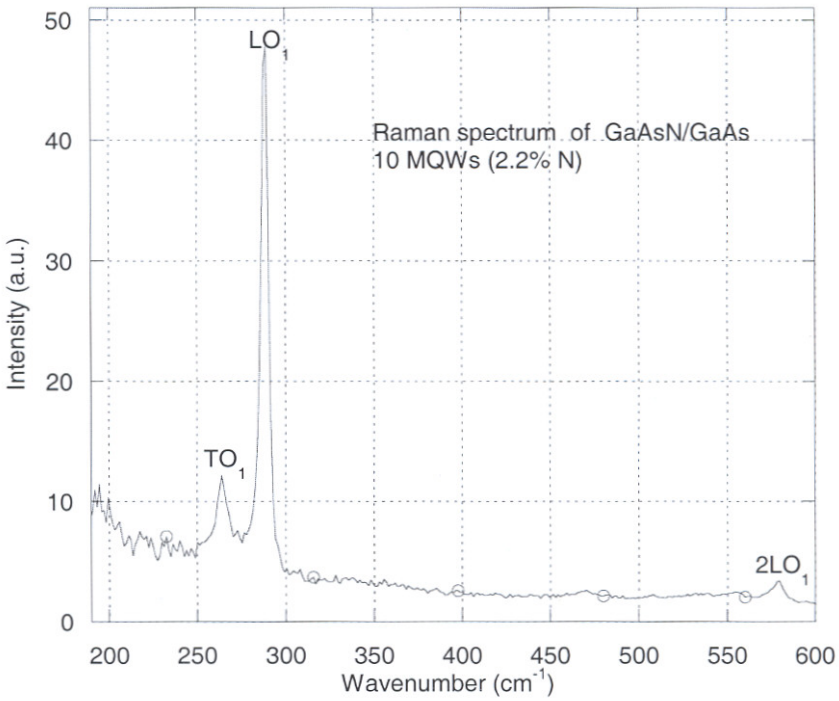

Figure 5.11: Room temperature Raman spectrum from a GaAsN/GaAs MQW sample with 2.2 % N

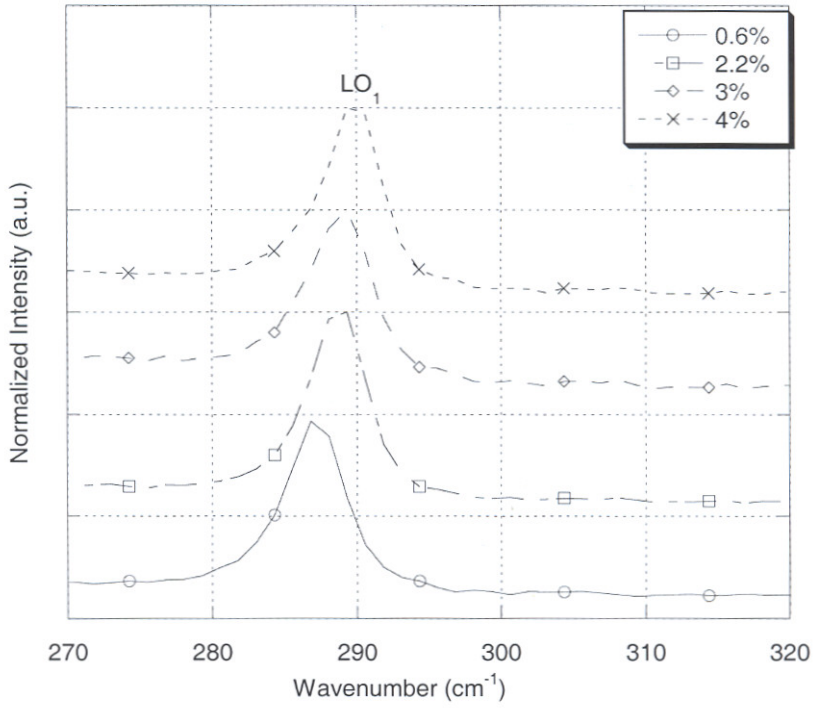

Figure 5.12: Spectra in the LO_1 range for varying nitrogen concentrations

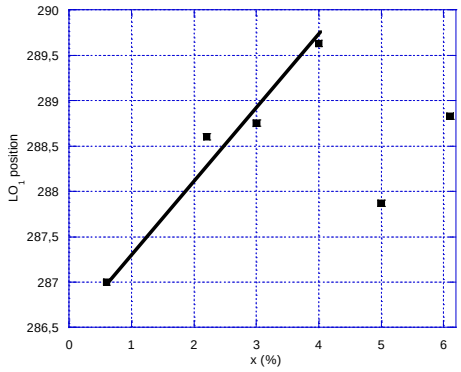

Figure 5.13: The shift of LO_1 phonons *vs.* nitrogen concentration

The LO_1 band frequency shifts to higher wavenumbers with increasing x for x <0.04. Fig. 5.13 displays the shift v(x$\leq$ 4%). A linear fit to the data results in a shift of 76.5 cm^{-1}/x. This shift is due to the effects of alloying and strain [85, 86]. It is 60 cm^{-1}/x smaller as compared to the results of Prokofyeva *et al.* [84]. According to their calculation, with the assumption that the deformation constants of GaAsN are the same as those of pure GaAs, the strain-only LO_1-mode phonon shift would be 96 cm^{-1}/x. This may be because there are less alloying phase transfers in our superlattice structure than that in the bulk epilayer in their measurements with increasing N concentration. The LO_1-phonon frequency of the sample with N concentration x>4% deviates from the linear trend, implying that strain relaxation occurred in these samples.

Summary We investigated the overall structural and optical properties of GaAsN/GaAs MQW samples with N concentrations of 0.6% to 6.1%.

The GaAsN/GaAs MQW samples were of good quality and exhibited sharp interfaces in the as-grown samples, as revealed by the XRD $2\theta - \omega$ pattern, Raman spectra and TEM images.

The PL emission quality is improved by RTA, as shown by a strongly enhanced intensity and reduced FWHM. The PL emission also shows a blue shift after RTA. One of the main reasons for this blue shift is proved to be atomic interface diffusion.

The S-shaped T-PL spectra show thermal emission of the carriers from localized states (caused by alloy composition fluctuations) to extended states as the measurement temperature increases.